Probing the folding capacity and residual structures in 1–79 residues fragment of staphylococcal nuclease by biophysical and NMR methods

Xu Wang, Min Wang, Yufeng Tong, Lu Shan, Jinfeng Wang [*]

National Laboratory of Biomacromolecules, Center for Structural and Molecular Biology, Institute of Biophysics, Chinese Academy of Sciences, 15 Datun Road, Beijing 100101, People's Republic of China

Abstract

1–79 residues SNase fragment (SNase79) has chain length containing a sequence for helix α_1, ω-loop, β_I-sheet, and partial β_{II}-sheet of native SNase. The incomplete "β-barrel" structural region of SNase79 makes this fragment to be interested in investigation of its conformation. For this study, we use CD, fluorescence, and NMR spectroscopy to probe the folding capacity and the residual structures in SNase79. The optical spectra obtained for SNase79 and its mutants reveal the presence of retained capacity for folding of the fragment. The NMR derived $^{13}C_\alpha$ secondary chemical shifts, $^3J_{NH-H\alpha}$ coupling constants, amide-proton temperature coefficients, interresidue NOEs, and ^{15}N relaxation data determine the intrinsic propensities for helix- and turn- or β-sheet-like conformations of SNase79, which is not the result of stabilizing inter-molecular interactions by oligomerization effects. The residual turn- and helix-like structures may serve as potential local nucleation sites, whereas the residual β_I-sheet-like structure can be regarded as a potential non-local nucleation site in the folding of SNase79. The intrinsic local and non-local interactions in these potential initiation sites are insufficient to stabilize the folding of SNase79 due to the shortage of relevant long-range interactions from other part of the fragment. The conformational ensemble of SNase79 is a highly heterogeneous collection of interconverting conformations having transiently populated helix- and β-sheet- or turn-like structures.
© 2006 Elsevier Masson SAS. All rights reserved.

Keywords: β-Sheet-like; Intrinsic propensities; Intrinsic interactions; Folding initiation sites; SNase79

1. Introduction

The information necessary for folding of polypeptide chain is contained in its amino acid sequence and the problem of protein folding in essence is how the amino acid sequence dictates the formation of tertiary structure of polypeptide. One approach to this problem is to use N-terminal fragments of increasing lengths of protein as a model system to study the development of structure on elongation of the chain lengths. Series of fragments of 64-residue chymotrypsin inhibitor 2 (CI-2) and 110-residue protein barnase of increasing size from their N-termini were studied by NMR spectroscopy and other biophysical methods. Studies of 10 N-terminal fragments of CI-2 demonstrated that the growing peptide chain has little tendency to form native-like structure until the size of fragment increases up to residues 1–53 [1,2]. Studies of the N-terminal fragments of barnase showed that the content of α-helical structure in the seven fragments was found to increase with increasing chain length while the fragments are disordered [3]. The results from both studies indicated that low levels of native-like secondary structure become stabilized by long-range interactions as folding proceeds.

Staphylococcal nuclease (Fig. 1) is a protein used widely in protein folding studies. We have used N-terminal fragments of staphylococcal nuclease (SNase) to explore the development of tertiary long-range interactions which is held as the determinant of the conformations taken by the fragments having different chain lengths [4–6]. The folding initiation sites of SNase were probed by characterization of the conformational states of three N-terminal short fragments of SNase, namely: SNase20, SNase28, and SNase36 containing residues 1–20, 1–28, and
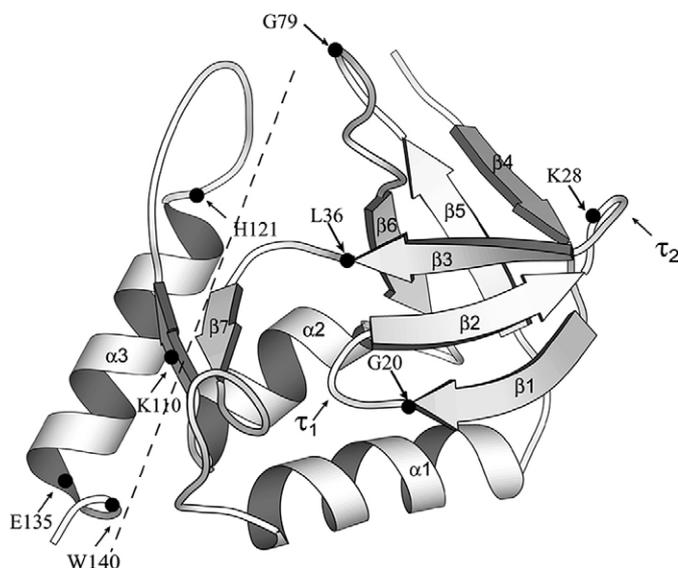

Fig. 1. Ribbon diagram representation of native staphylococcal nuclease using the program MOLSCRIPT. Arrowheads indicate the approximate positions of the truncation sites for the fragments used in the studies. The three α-helices (α$_1$: 58–69, α$_2$: 98–106; α$_3$: 122–136), six β-strands in the "β–barrel" region (β$_4$: 8–12; β$_1$: 13–17; β$_2$: 22–26; β$_3$: 31–35; β$_5$: 72–76; β$_6$: 90–93), and two turns (τ$_1$: 18–21; τ$_2$: 27–30) are labeled.

1–36, respectively. The transient population of bend-like conformation at A12–L14 and the populated localized structural propensities for turn-like conformations at residues A17–T22 and Y27–Q30 were observed correspondingly for SNase20, SNase28, and SNase36, which may serve as the folding nucleation sites for SNase fragments [4]. Conformational features of the N-terminal large fragments of SNase, SNase110 (residues 1–110), SNase121 (residues 1–121), SNase135 (residues 1–135), and SNase140 (residues 1–140), and the G88W- and V66W-mutant fragments, G88W110, G88W121, V66W110, and V66W121 revealed the folding pathways of SNase fragments of increasing lengths from the N-terminus. The increase in native-like tertiary fold and enzyme activity is concomitant, and follows the development of native-like tertiary interactions in the fragments as the chain length increases. Promoting the tertiary interactions of the fragments by G88W and V66W mutations drives the fragments to fold into more stable native-like β-subdomain [5]. A 1–44 residues fragment of SNase was generated by chemical cleavage and no stable pairing between strand segments β$_1$, β$_2$, and β$_3$ was observed as would be expected for a native-like β-sheet [7]. Studies of G88W and V66W-mutant fragments containing 1–102 residues (G88W102 and V66W102) estimated that 40% and 30% of the G88W102 and V66W102 molecule, respectively, are structured in solution [6]. G88V/V66L double mutations of the fragment containing 1–103 residues provide a stable and cooperative "β-barrel" conformation, which is a main hydrophobic core of SNase [8]. The 1–102 (or 1–103) residues SNase fragment comprises the integrated "β-barrel" and helix α$_1$ structural regions. In contrast, 1–44 residues SNase fragment has a shortage of helix α$_1$ and one of the two β-sheets in the "β-barrel" region. The great differences in sequences between these two

fragments determine their different long-rang interactions and conformations. It will be interesting to detect the folding behavior of a SNase fragment which has sequence incomplete for the "β-barrel" structural region.

SNase79 covers the sequences of structural elements: two β-turns (τ$_1$: I18–D21 and τ$_2$: Y27–Q30), helix α$_1$ (A58–A69), ω-loop (P42–E57), β$_I$-sheet (T13–R35) and strands β$_4$ (H8–P11), β$_5$ (I72–F76), and β$_7$ (V39–T41) for native SNase [9] (Fig. 1). Lacking strand β$_6$ (A90–Y93), SNase79 has an incomplete sequence for "β-barrel" structural region of native SNase, which is formed by β$_I$-sheet consisting of strands β$_1$, β$_2$, and β$_3$ and β$_{II}$-sheet consisting of strands β$_4$, β$_5$, and β$_6$. The previous study has indicated that a large population of SNase79 has strong tendency to aggregate and a small population of SNase79 is in monomeric state, relating to the *trans*- and *cis*-forms of the X-prolyl bond Q30–P31, respectively [10]. In this study, the localized structural propensities, residual structures, and conformational features of SNase79 are probed by CD, fluorescence, and NMR spectroscopy. The studies were carried out with a variety of SNase79 samples. A group of NMR data are presented and used for probing the intrinsic interactions in SNase79.

2. Materials and methods

2.1. Sample preparation

The natural SNase79 and uniformly ^{15}N and ^{15}N/^{13}C-labeled SNase79 were expressed and purified as previously described [10]. The plasmid constructions for V66W-mutant 79-residue fragment (V66W79) were achieved by polymerase chain reaction (PCR) of the genes of V66W110 [6]. The PCR products were inserted into the NdeI and BamHI sites of plasmid pET-3a, and were sequenced to confirm the presence of the desired mutation. The G20V/G29V double mutant fragment, [G20V/G29V]SNase79, was created using QuickChange Site-Directed Mutagenesis Kit (Stratagene, La Jolla, CA, USA) [11]. The complementary primers (G20V-1 and Antisence G20V-2; G29V-1 and Antisence G29V-2) were designed with the desired mutations. The [G20VG29V]SNase79 plasmid was generated through PCR reaction using pET3a-SNase79 as template. A 5.0 μl aliquot of the above PCR product was used to transform TOP10 chemically competent cells and sequenced to confirm the presence of the desired mutation.

2.2. Far-UV CD measurements

Circular dichroism experiments were performed on a Jasco 720 spectropolarimeter at 298 K. Rectangular cell with path lengths of 1 mm was employed to record the spectra in the wavelength range of 190–250 nm. Four scans were averaged for each measurement. The samples for CD measurements were 15 μM SNase79 in 0, 2.0, 4.0, and 6.0 M urea; 15 μM SNase79 in 0.5, 1.0, 1.5, 2.0, 2.5, 3.0, 4.0, and 5.0 M TMAO; 50 μM SNase79 in H$_2$O. All sample solutions contained 25 mM Tris–HCl buffer (pH 7.0).

2.3. Steady state fluorescence measurements

Fluorescence intensity was measured by a Hitachi F-4500 spectrophotofluorometer at 298 K. All spectra were acquired using the same excitation and emission slit widths of 5 nm. For the intrinsic tyrosine fluorescence experiments the excitation wavelength was fixed at 278 nm, and the emission was monitored in the wavelength range of 290–330 nm. The samples for tyrosyl intrinsic fluorescence measurements were 5 μM SNase79 in aqueous solution and in the presence of either 2.0 M TMAO or 6.0 M urea. The ANS-binding fluorescence experiments were performed at excitation wavelength of 345 nm with 5 μM SNase79 in 50 μM 1, 8-ANS and in both 50 μM 1, 8-ANS/6.0 M urea and 50 μM 1, 8-ANS/2.0 M TMAO mixtures. Acrylamide quenching studies of intrinsic fluorescence were performed by adding aliquots from the stock solution of acrylamide into the fluorescence cuvette containing sample solution, which was 15 μM SNase79 in aqueous solution and in 2.0 M TMAO. The fluorescence quenching data were analyzed according to the classic Stern–Volmer equation ($F_0/F = (1 + K_{sv}[Q])\exp(V[Q])$), where F_0 and F are the fluorescence intensities in the absence and presence of quencher, $[Q]$ is the concentration of the quencher and K_{sv} is the Stern–Volmer quenching constant obtained from the slope of a plot of F_0/F versus $[Q]$ [12].

2.4. Nuclear magnetic resonance spectroscopy

All NMR spectra were acquired at 300 K with Bruker DMX 600 spectrometer equipped with a triple-resonance cryo-probe. 3D heteronuclear NMR experiments carried out in this study are as follows: 3D ^1H_N–^{13}C–^{15}N HNCA, HN(CO)CA, HNCACB, and CACB(CO)NH experiments for backbone resonance assignment; 3D ^1H_N–^{15}N HNHA experiment for $^3J_{HN–H\alpha}$ coupling constant measurement; 3D ^1H_N–^{15}N TOCSY-HSQC and NOESY-HSQC experiments for side chain and NOE assignments. The 3D ^1H_N–^{15}N NOESY-HSQC spectrum was recorded at mixing time of 150 ms. 2D ^1H_N–^{15}N HSQC experiments were run for SNase79 at different protein and urea concentrations, and at different temperatures. The 2D ^1H_N–^{15}N HSQC spectra for determination of ^1H_N temperature coefficient were collected in the temperature range from 292.5 to 304.5 K at increment of 1.5 K. Two type samples were used for above multidimensional NMR experiments. They are SNase79 in 90% H_2O/10% D_2O containing protein of various concentrations and 20 mM d_4-acetate buffer (pH 4.9), and SNase79 in urea having different protein and urea concentrations. For relaxation study, the 2D ^{15}N R_1 and R_2 experiments were carried out at 300 K. The delay times for ^{15}N R_1 measurements were set to 20, 40, 50, 60, 80, 100, 120, 140, 160, 180, 200, and 220 ms for 50 μM SNase79 and 30, 100, 150, 200, 250, 300, 400, 600, and 700 ms for 400 μM SNase79 in 4.0 M and 6.0 M urea. For R_2 measurements, the relaxation delays were 8.48, 16.96, 25.44, 33.92, 42.4, 50.88, 59.6, 67.84, 76.32, 84.8, 93.28, and 101.76 ms with a spin echo delay of 900 μs for 50 μM SNase79 in aqueous solution and 16.96,

67.84, 84.8, 101.76, 135.68, 152.64, 169.6, and 186.56 ms with a spin echo delay of 900 μs for 400 μM SNase79 in 4.0 M and 6.0 M urea. The samples used for various NMR experiments are summarized in Table 1. All NMR data were processed and analyzed using FELIX98 (MSI/Accelrys Inc). The data points in each indirect dimension were usually doubled by linear prediction before zero filling to the appropriate size. ^1H chemical shifts were referenced to DSS at 0 ppm. ^{15}N and ^{13}C chemical shifts were referenced indirectly [13].

3. Results

3.1. Residual secondary structures inferred by CD spectra

The far-UV CD spectrum of 15 μM SNase79 in aqueous solution showed a pronounced and shallow minimum at approximately 200 and 220 nm, respectively (Fig. 2a). The pronounced minimum at about 200 nm is a characteristic of non-ordered conformation of SNase79 in aqueous solution. Adding urea into sample solution decreased the ellipticity at about 220 nm, and 6.0 M urea eliminated entirely this minimum. Fig. 2b shows the differences in the ellipticities obtained in the wavelength range from 210 to 250 nm by subtracting the CD spectra of 15 μM SNase79 in the presence of 2.0, 4.0, and 6.0 M urea from those of 15 μM SNase79 in aqueous solution. The increased differences in ellipticities on increasing the urea concentrations demonstrated that a small population of residual secondary structures may exist in SNase79.

Far-UV CD spectra of SNase79 in the presence of a wide range of TMAO concentrations indicated that 2.0 M TMAO is high enough to complete conformational transition of SNase79 (Fig. 1 in supplementary materials). In the presence of 2.0 M TMAO, the far-UV CD spectrum of 15 μM SNase79 demonstrated an increase in negative ellipticity in region 210–230 nm compared to those of SNase79 in aqueous solution, showing the increase of structural content (Fig. 2a). This evidenced again the existence of residual structure in SNase79, since TMAO can increase the unfolding free energy of denatured protein [14]. Analysis of the CD spectra using program CONTIN in the software package CDPro (http://lamar.colostate.edu/~sreeram/CDPro) gave approximately 15.4% α-helix, 33.4% β-sheet, and 22.0% turn for SNase79 in aqueous solution.

3.2. Fluorescence spectra indicate residual β-sheet or turn structures

1,8-ANS was used as a hydrophobic fluorescence probe [15, 16] to study the changes in solvent-exposed hydrophobic surfaces of SNase79. Dramatic increase in the ANS-binding fluorescence intensity and a blue shift of the fluorescence maximum were obtained for SNase79 in the presence of 2.0 M TMAO (Fig. 3a). This suggests that the solvophobic effect of TMAO [14] induces a certain degree of folding of SNase79 and a loosely packed solvent-accessible hydrophobic patch may be formed in SNase79, increasing greatly the affinity of ANS to

Table 1
Summary of the samples used for various NMR experiments

Experiments	Samples	Figures
For backbone resonance assignment		
3D ^{1}H/^{13}C/^{15}N HNCA and HN(CO)CA	500 μM SNase79 in aqueous solution[a]	
	400 μM SNase79 in 3.0 and 6.0 M[a] urea	
3D ^{1}H/^{13}C/^{15}N HNCACB and CBCACONH	400 μM SNase79 in aqueous solution	7b[b]
	400 μM SNase79 in 6.0 M urea[a]	
For side chain resonance and NOE assignment		
3D ^{1}H$_N$–^{15}N TOCSY-HSQC	500 μM SNase79 in aqueous solution	
	400 μM SNase79 in 6.0 M urea	
3D ^{1}H$_N$–^{15}N NOESY-HSQC	500 μM SNase79 in aqueous solution,	7a[c]
	400 μM SNase79 in 4.0 M urea	
For $^3J_{HN-H\alpha}$ coupling constants measurement		
3D ^{1}H$_N$–^{15}N HNHA	500 μM SNase79 in aqueous solution	5
	400 μM SNase79 in 4.0 M urea	
For urea-denaturation study		
2D ^{1}H$_N$–^{15}N HSQC	400 μM SNase79 in 1.0, 2.0, 3.0, 4.0, 5.0 and 6.0 M urea	8b, c, d
For concentration dependent study		
2D ^{1}H$_N$–^{15}N HSQC	5, 15, 50, 100, 200, 250, 350, 500, and 1000 μM SNase79 in aqueous solution	8a
For ^{1}H$_N$ temperature coefficient measurement		
2D ^{1}H$_N$–^{15}N HSQC	50 μM SNase79 in aqueous solution	6
For backbone relaxation measurement		
2D ^{1}H$_N$–^{15}N R_1 and R_2 and ^{1}H$_N$–^{15}N NOE	50 μM SNase79 in aqueous solution	9
	500 μM [G20V/G29V]SNase79 in aqueous solution	
	400 μM SNase79 in 4.0 M and 6.0 M urea	
2D ^{1}H$_N$–^{15}N HSQC	50 μM SNase79 in aqueous solution	4a
	400 μM SNase79 in 1.0 M urea	4b
	500 μM [G20V/G29V]SNase79 in aqueous solution	4c
	15 μM V66W79 in aqueous solution	4d

[a] For backbone resonance assignment of SNase79 in 6.0 M urea.
[b] The experiments with these samples provided the assignments for backbone ^{13}C$_\alpha$ resonances.
[c] Only the NOEs obtained for 500 μM SNase79 in aqueous solution were indicated in the figure.

SNase79. The 6.0 M urea eliminated the ANS-binding affinity of SNase79 as a result of fully unfolding of SNase79.

The tyrosyl intrinsic fluorescence can monitor conformational changes in the environment of tyrosine residue [17]. The explicit decrease and apparent increase in the intrinsic fluorescence intensity were observed for SNase79 in the presence of 2.0 M TMAO and 6.0 M urea, respectively, as compared with those of SNase79 in aqueous solution (Fig. 3b). This reflects the changes in local environment of Y27 in the β-turn τ$_2$ of native SNase, since another tyrosine residue of SNase79 (Y54) is located in the flexible ω-loop of native SNase. Fig. 3b reveals that side chain of Y27 is more buried for SNase79 in 2.0 M TMAO and more exposed for SNase79 in 6.0 M urea. The environment-driven changes in the accessibility of Y27 were further detected by the acrylamide quenching of intrinsic fluorescence of SNase79 in 0 and 2.0 M TMAO. The Stern–Volmer plots (Fig. 2 in supplementary materials) provided the K_{sv} values of 26.93 ± 3.54 M^{-1} and 17.44 ± 2.28 M^{-1} for SNase79 in 0 and 2.0 M TMAO, respectively. This indicates that the side chain of Y27 is partially protected from quencher molecule as a result of the changes in its local conformation at 2.0 M TMAO, suggesting the existence of some retained folding capacity for forming residual structures in SNase79. Therefore, the ANS-binding and tyrosyl intrinsic fluorescence spectra of monomeric SNase79 in the presence and absence of TMAO or urea give evidences for the residual β-sheet or turn structures in the fragment.

3.3. NMR derived data describing the conformation of SNase79

3.3.1. NMR resonance assignment

The backbone ^{1}H$_N$ and ^{15}N resonance were assigned for 400 μM SNase79 in aqueous solution and in 3.0 M urea using the 3D heteronuclear NMR experiments, whereas those for 50 and 500 μM SNase79 in aqueous solution and 400 μM SNase79 in 6.0 M urea were identified previously [10]. The cross peaks in the 2D ^{1}H$_N$–^{15}N HSQC spectra of 400 μM SNase79 in 1.0, 2.0, 4.0, and 5.0 M urea showed a distribution pattern very close to those of 400 μM SNase79 in 3.0 and 6.0 M urea. Thus, the ^{1}H$_N$ and ^{15}N resonances in the spectra of 400 μM SNase79 in 1.0, 2.0, 4.0, and 5.0 M urea can be assigned with reference to the obtained assignments for 400 μM SNase79 in 3.0 and 6.0 M urea. The dispersion of the ^{1}H$_N$–^{15}N cross-peaks in the 2D ^{1}H$_N$–^{15}N HSQC spectrum of 50 μM SNase79 in aqueous solution is very similar to those of 400 μM SNase79 in the presence of urea. This can be seen in Fig. 4a, b, showing the spectral similarity of 50 μM SNase79 in aqueous solution to 400 μM SNase79 in 1.0 M urea. Therefore, the above identified assignments can be used for analysis the NMR data in this study, and the concerns over oligomerization effects of SNase79 at high concentrations can be excluded. The assignments for SNase79 in aqueous solution at protein concentrations of 5, 15, 100, 200, 250, 350, and 1000 μM are
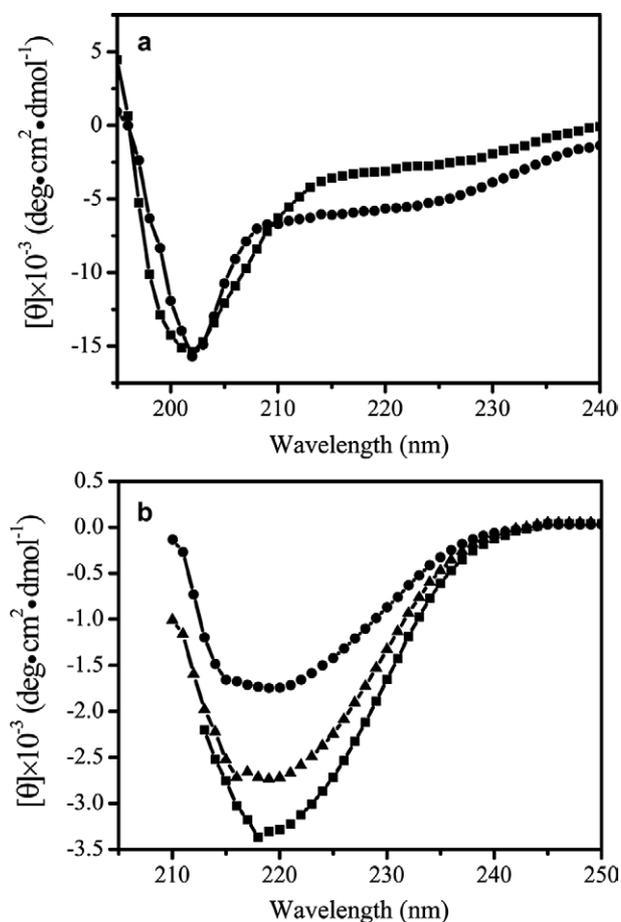
Fig. 2. Far-UV CD spectra of SNase79 recorded at 298 K. (a) Spectra for 15 μM SNase79 in aqueous solution (■) and in the presence of 2.0 M TMAO (●). (b) Differences of the ellipticities between the spectra of 15 μM SNase79 in aqueous solution and those in the presence of urea: (●) H₂O–2.0 M urea; (π) H₂O–4.0 M urea; (■) H₂O–6.0 M urea.
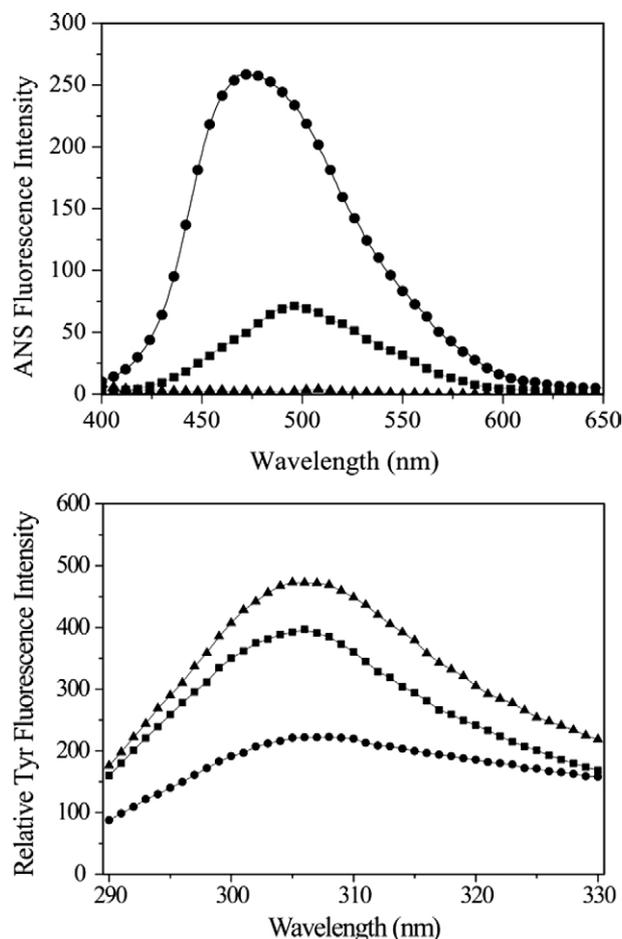

Fig. 3. (a) Fluorescence emission spectra of 1, 8-ANS for 5 μM SNase79 under different conditions. (b) Relative intensity in tyrosyl fluorescence of 5 μM SNase79 under different conditions. SNase79 samples were prepared in aqueous solution (■), in 2.0 M TMAO (●), and in 6.0 M urea (π).

readily obtained in comparison with those for 50, 400, and 500 μM SNase79 in aqueous solution, since they provide similar 2D ^1H_N–^{15}N HSQC spectra. The $^{13}C_\alpha$ resonances of 400 μM SNase79 in the absence and presence of 6.0 M urea were assigned by analysis of the 3D heteronuclear NMR data.

3.3.2. $^3J_{NH–H\alpha}$ coupling constants predicting secondary structures

$^3J_{NH–H\alpha}$ coupling constant as one of the NMR parameters for detecting the backbone conformation can provide a basis for analyzing conformational preferences along the polypeptide chain. The distributions of $^3J_{NH–H\alpha}$ coupling constants for different secondary structures were predicted from the protein data base. For residues in segment of helix (or turn) and β-strand, the $^3J_{NH–H\alpha}$ values are mainly distributed in the ranges of 3.0–7.0 Hz and 7.0–10.0 Hz, respectively [18]. The average of $^3J_{NH–H\alpha}$ values for model random coil is around 7.0 Hz. Thus, residues having $^3J_{NH–H\alpha}$ values significantly above and below the average may tend to form β-strand-like and helical-like (or turn-like) structures, respectively. For extracting the information to determine the $^3J_{NH–H\alpha}$ coupling constants from the 3D ^1H_N–^{15}N HNHA spectrum [19], 500 μM SNase79 in

aqueous solution and 400 μM SNase79 in 4.0 M urea were used in the experiments. The experimentally obtained $^3J_{NH–H\alpha}$ coupling constants for residues of SNase79 were grouped by amino acid type in Fig. 5.

Resonance signals for residues in association region T13–V39 were eliminated by aggregation of SNase79 at concentration of 500 μM [10]. The $^3J_{NH–H\alpha}$ values were determined for 20 residues of 500 μM SNase79 (Fig. 5a). Fourteen out of 20 residues provided the determined $^3J_{NH–H\alpha}$ values having non-negligible deviations (≥±0.7 Hz) from random coil values. Among them residues E57, A58, A60, F61, T62, M65, and V66 forming helix α_1 and T44 and K49 in loop region of native SNase showed the $^3J_{NH–H\alpha}$ values within 3.0–7.0 Hz. Residues D77 and G79 at the c-terminal of SNase79 and T41 from strand V39–D40–T41 showed the $^3J_{NH–H\alpha}$ values within 7.0–10.0 Hz. Residue G52 in loop region of native SNase has a value very close to 7.0 Hz.

Denaturant urea can release SNase79 of high concentration from self-association, and 400 μM SNase79 can provide the resonance signals of residues T13–V39 in the presence of 4.0 M urea. Fig. 5b shows the $^3J_{NH–H\alpha}$ values for 33 residues of 400 μM SNase79 in 4.0 M urea. Twenty-five out of 33 resi-
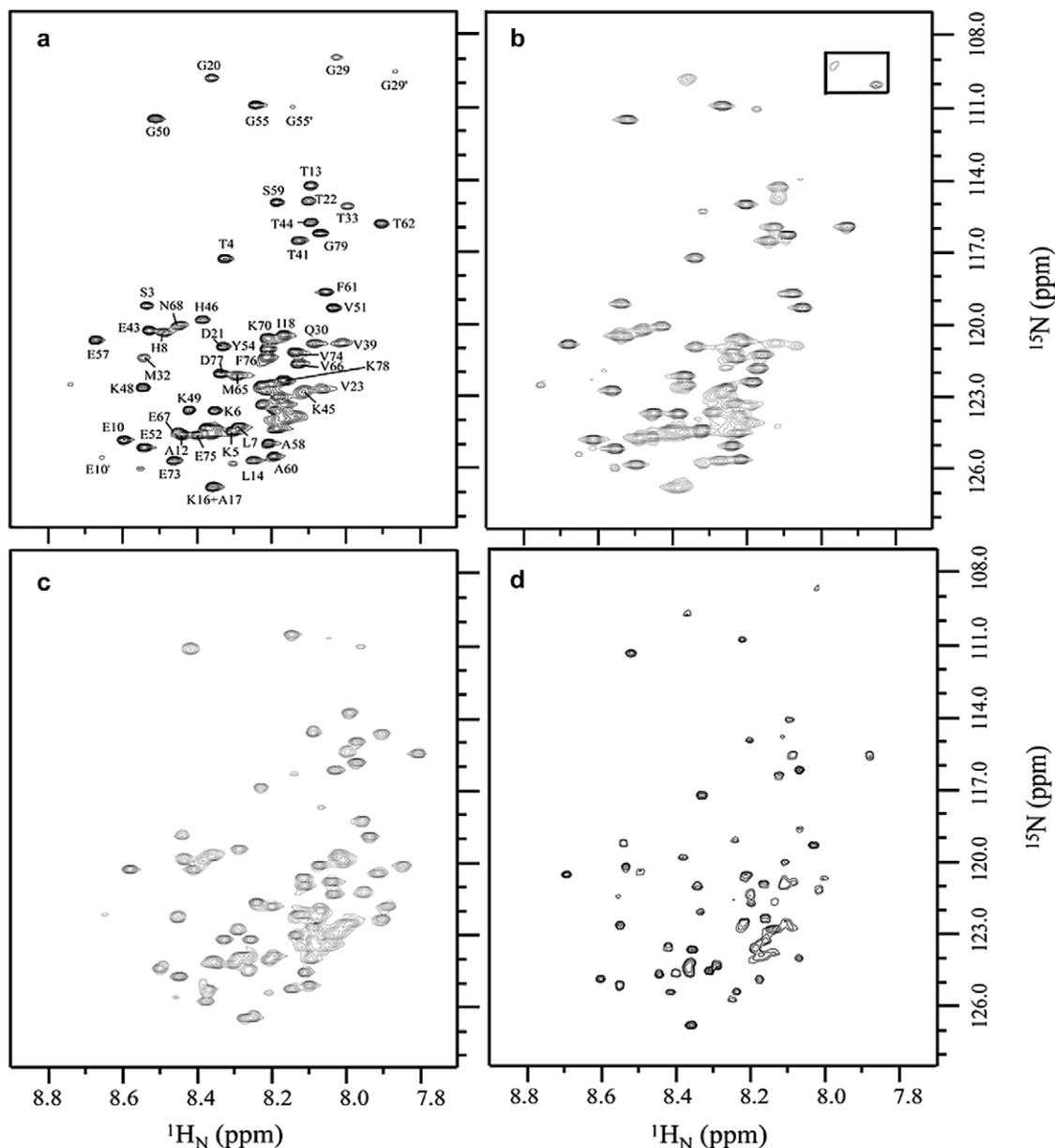
Fig. 4. 2D ^1H_N–^{15}N HSQC spectra of 50 μM SNase79 in aqueous solution (a), 400 μM SNase79 in 1.0 M urea (b), 500 μM [G20V/G29V]SNase79 in aqueous solution (c), 15 μM V66W79 in aqueous solution (d). Resonance assignments are indicated in (a) with residue number and one-letter amino acid code. The cross-peaks in small box in (b) were plotted with low contour levels.

dues showed $^3J_{NH–Hα}$ values with non-negligible deviations (≥ ±0.7 Hz) from the random coil values. For residues A58, S59, F61, T62, and K64 forming helix $α_1$ and residues I18, Q30, and K48 in turn or loop regions of native SNase, the $^3J_{NH–Hα}$ values were distributed in the range of 3.0–7.0 Hz. Residues G20 and G29 in turn regions of native SNase showed $^3J_{NH–Hα}$ values close to 7.0 Hz. The $^3J_{NH–Hα}$ values of residues K16, A17, D21, Y27, M32, E73, and V74 from the "β-barrel" structural region and some residues from loop region in native SNase were distributed in the range of 7.0–10.0 Hz.

The most detected $^3J_{NH–Hα}$ values for residues of 500 μM SNase79 in aqueous solution and 400 μM SNase79 in 4.0 M urea are spread over the predicted ranges. The residues in

α-helix and β-sheet or turn regions of native SNase, having the $^3J_{NH–Hα}$ values within 3.0–7.0 Hz or 7.0–10.0 Hz for 500 μM SNase79 in aqueous solution, showed also the $^3J_{NH–Hα}$ values in the corresponding ranges for 400 μM SNase79 in 4.0 M urea. In the presence of 4.0 M urea, the detected $^3J_{NH–Hα}$ values can indicate the retained tendency for secondary structures of 400 μM SNase which is in monomeric state in this case. Therefore, the identified residues having the $^3J_{NH–Hα}$ values in the predicted distribution ranges for both 500 μM SNase79 in aqueous solution and 400 μM SNase79 in 4.0 M urea may predict directly the localized backbone conformations exhibiting the helix-, β-strand-, and β-turn-like structures for SNase79 in monomeric state.
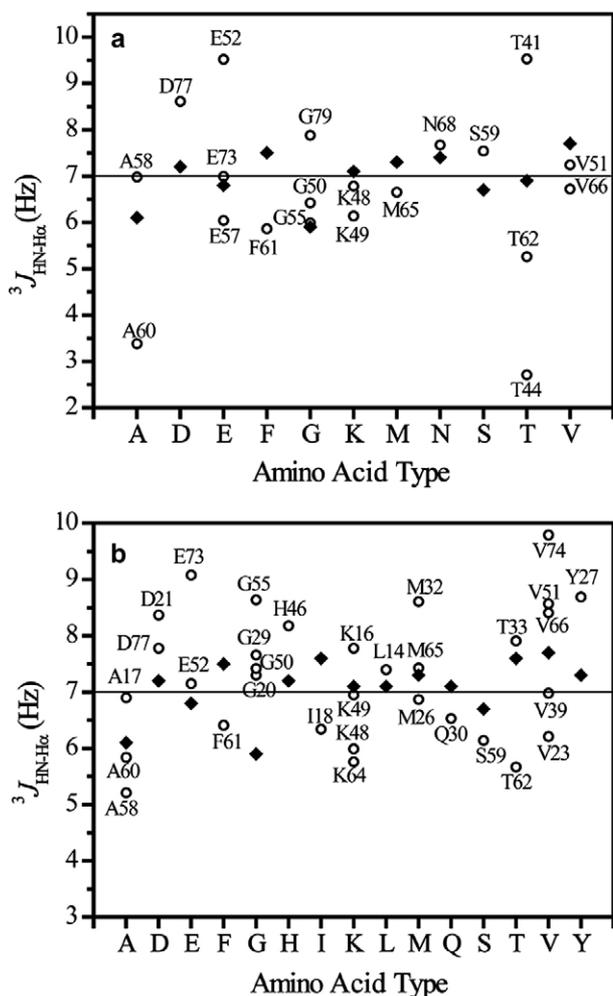
Fig. 5. $^3J_{NH-H\alpha}$ coupling constants for 500 μM SNase79 in aqueous solution (a) and 400 μM SNase79 in the presence of 4.0 M urea (b). The $^3J_{NH-H\alpha}$ coupling constants are arranged according to residue type. The filled diamonds denote the values predicted from the random coil model. The open circles denote the values for residues of SNase79.

3.3.3. Estimation of hydrogen bonding by ^1H_N temperature coefficients

Amide proton temperature coefficient ($\Delta\delta/\Delta T$) provides an ideal measure of the involvement of the amide proton in hydrogen bonding [20]. A small temperature coefficient indicates the amide proton under the protection of hydrogen bonding from the interaction of solvent molecules. In general, a value of $\Delta\delta/\Delta T$ more positive than –4.5 ppb K^{-1} is used as an indicator for intramolecular hydrogen bonding [21]. $\Delta(\Delta\delta/\Delta T)$ was defined as a deviation of $\Delta\delta/\Delta T$ value of amide proton from those of the corresponding amide proton in random coil. As was suggested, amide proton having a value of $\Delta(\Delta\delta/\Delta T) \geq 1$ ppb K^{-1} may involve, at least transiently, in either intramolecular or intermolecular hydrogen bonding [22,23]. $\Delta\delta/\Delta T$ of SNase79 were obtained for ^1H_N chemical shifts of the assigned cross peaks in the 2D ^1H_N–^{15}N HSQC spectra collected for 50 μM SNase79 in aqueous solution over the experimental temperature range. Fig. 6a, b show the estimated $\Delta\delta/\Delta T$ and $\Delta(\Delta\delta/\Delta T)$ values, respectively, for ^1H_N of resolved cross peaks from 38 out of 79 amino acid residues of SNase79.
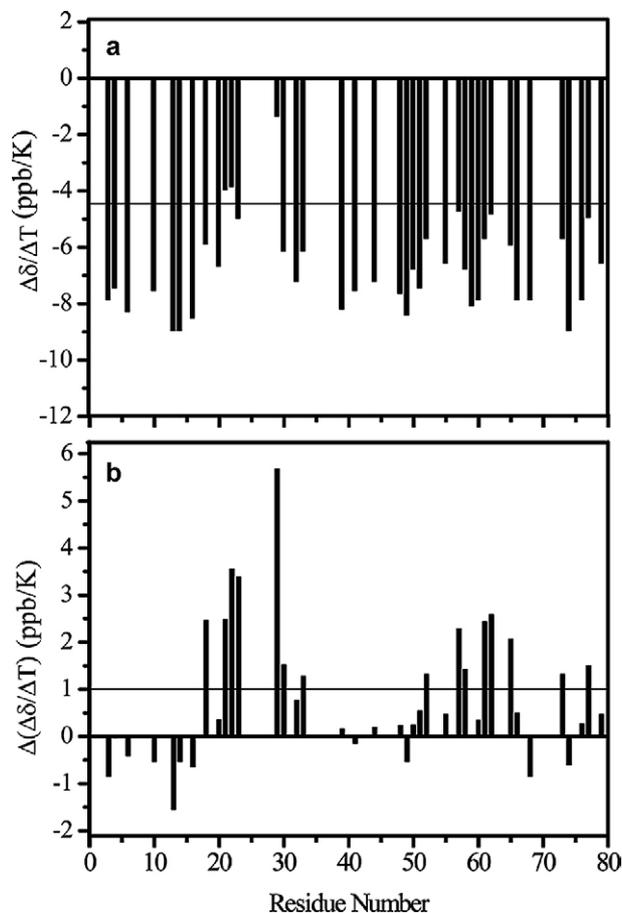

Fig. 6. Amide proton temperature coefficients versus sequence of SNase79. (a) Temperature coefficient, $\Delta\delta/\Delta T$, (b) Deviations of $\Delta\delta/\Delta T$ for SNase79 from their random coil values, $\Delta(\Delta\delta/\Delta T)$.

The estimated temperature coefficients for SNase79 revealed that fifteen residues were supposed to involve in either intramolecular or intermolecular hydrogen bonding, since their $\Delta(\Delta\delta/\Delta T) \geq 1$ ppb K^{-1} (Fig. 6b). They are residues in β_I-sheet: I18, D21, T22, V23, G29, Q30, and T33, residues in helix α_1: E57, A58, F61, T62, and M65, and residues in other regions: E52, E73, and D77. Residues D21, T22, and G29 located in turn regions of β_I-sheet in native SNase are more likely involved in intramolecular hydrogen bonding (Fig. 6a). The self-association reaction can be excluded essentially in aqueous solution for SNase79 at concentration of 50 μM [10], therefore the above indicated residues are supposed to built hydrogen bonds with residues in the same SNase79. Since most of theses residues are centralized in sequences corresponding to secondary structural regions of native SNase, their involvement in intramolecular hydrogen bonding can reflect the residual β-sheet and α-helix or turn structures of SNase79 in monomeric state.

3.4. Helical conformation suggested by $^{13}C_\alpha$ secondary chemical shifts

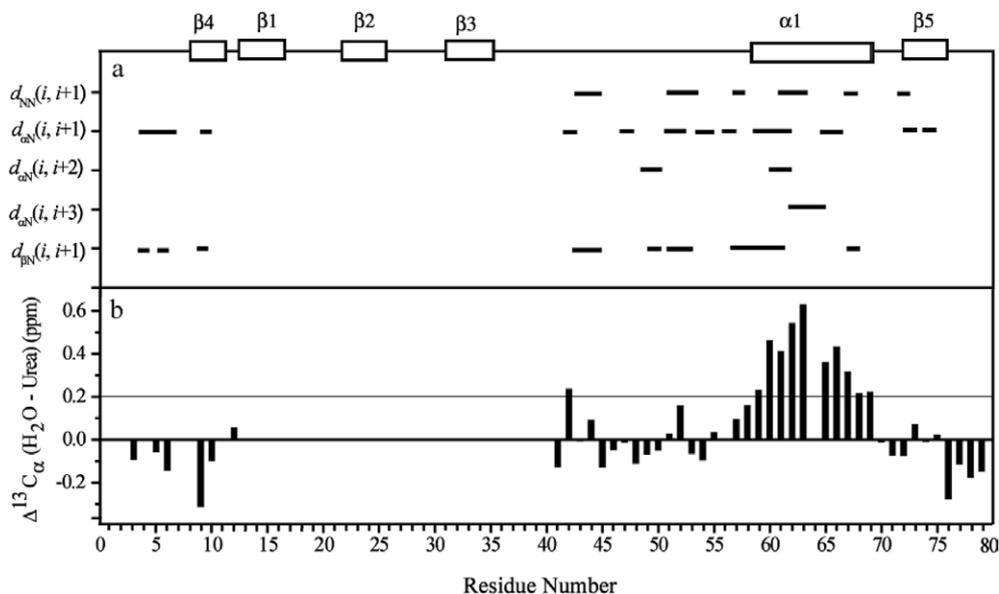SNase79 contains the complete sequence for helix α_1 of native SNase [9,24]. The NOE connectivity can be used to

Fig. 7. NOE connectivities identified for 500 SNase79 in aqueous solution (a). (b) Differences in chemical shifts of backbone $^{13}C_\alpha$ resonances for 400 μM SNase79 in aqueous solution form those for 400 μM SNase79 in 6.0 M urea. The elements of secondary structure for native SNase are indicated at the top of the figure.

detect the residual helix structure in SNase79. Considering the experimental sensitivity, 500 μM SNase79 in aqueous solution and 400 μM SNase79 in 4.0 M urea were used in the 3D ^1H_N–^{15}N NOESY-HSQC experiments. At high protein concentrations, the self-association reaction of SNase79 tends to eliminate the resonance signals for residues in the association region T13–V39. Thus, the NOE cross-peaks are expected to observe for residues T2–A12 and T41–G79 of 500 μM SNase79 in aqueous solution. Most identified NOE connectivities are sequential. A few medium-range NOE connectivities were obtained. Among them $d_{\alpha N}(i, i + 2)$ NOEs were obtained for pairs of residues K48–G50 and A60–T62 and $d_{\alpha N}(i, i + 3)$ NOE for T62–M65 (Fig. 7a). Since residues A58–A69 are not involved in the self-association reaction of SNase79, the obtained medium range $d_{\alpha N}(i, i+2)$ and $d_{\alpha N}(i, i + 3)$ NOEs for pairs of residues A60–T62 and T62–M65 are the intramolecular but not the intermolecular NOEs. This may imply a tendency for formation of the localized helical conformation of the sequence A58–A69 in monomeric SNase79. However, most of the residues of 400 μM SNase79 in 4.0 M urea showed only the sequential $d_{\alpha N}$, d_{NN}, and $d_{\beta N}$ NOEs (spectrum not shown), which characterizes a conformational averaging in a random coil ensemble of polypeptide chain.

The $^{13}C_\alpha$ secondary chemical shifts can be used to verify helix-forming tendency, because $^{13}C_\alpha$ chemical shifts have been shown to be highly sensitive to backbone torsion angles imposed by regular secondary structures [25,26]. The assignments for $^{13}C_\alpha$ resonances were obtained from the 3D heteronuclear NMR experiments carried out with 400 μM SNase79 in the absence and presence of 6.0 M urea. The polypeptide chain of SNase79 in 6.0 M urea behaves as a random coil. Thus, the deviation in $^{13}C_\alpha$ chemical shifts obtained by subtracting the $^{13}C_\alpha$ chemical shifts of 400 μM SNase79 in 6.0 M urea from those in aqueous solution, namely $\Delta^{13}C_\alpha$ (H_2O–6.0 M urea), can be regarded as secondary chemical

shifts for predicting a local preference for certain α-helical conformation in SNase79. Fig. 7b shows the $\Delta^{13}C_\alpha$ (H_2O–6.0 M urea) values along the sequence of SNase79. It should be noticed that aggregation of SNase79 at concentrations of 400 μM in aqueous solution makes the assignment of $^{13}C_\alpha$ resonances of the residues T13–V39 unobtainable. The assigned $^{13}C_\alpha$ chemical shifts for residues other than T13–V39 provided a "dense" group of positive $\Delta^{13}C_\alpha$ for residues A58–A69. Usually, the $^{13}C_\alpha$ resonances for residues in α-helix show downfield shifts about 2.6 ppm from the random coil value. Therefore, the localized helical conformation of segment A58–A69 can be postulated to populate transiently in the conformational ensemble of SNase79, since the $^3J_{NH–H\alpha}$ values measured for 500 μM SNase79 in aqueous solution can predict also the residual helical conformation in sequence A58–A69.

3.5. Native-like β-turn conformation affirmed by urea-denaturation experiment

As was analyzed in the previous study [10], SNase79 involving in aggregation at concentrations higher than 100 μM exhibits high population in aqueous solution. The explicit decrease in intensity ratio of cross-peaks for residues T13–V39 but not for other residues on increasing protein concentrations depicted the self-association interface for aggregated SNase79 (Fig. 8a). However, [G20V/G29V]SNase79 at concentration of 500 μM did not undergo self-association reaction, since its 2D ^1H_N–^{15}N HSQC spectrum showed the cross-peaks for majority residues in sequence region T13–V39 (Fig. 4c) compared to 50 μM SNase79 in aqueous solution (Fig. 4a). In contrast, V66W79 showed similar spectrum to those of SNase79 at low protein concentration (Fig. 4d), but aggregated at high protein concentration (spectrum not shown). G29 and G20 are residues located in β-turn τ_2 and τ_1, respectively, for native SNase. Usually, β-turn structure requires a glycine residue at the
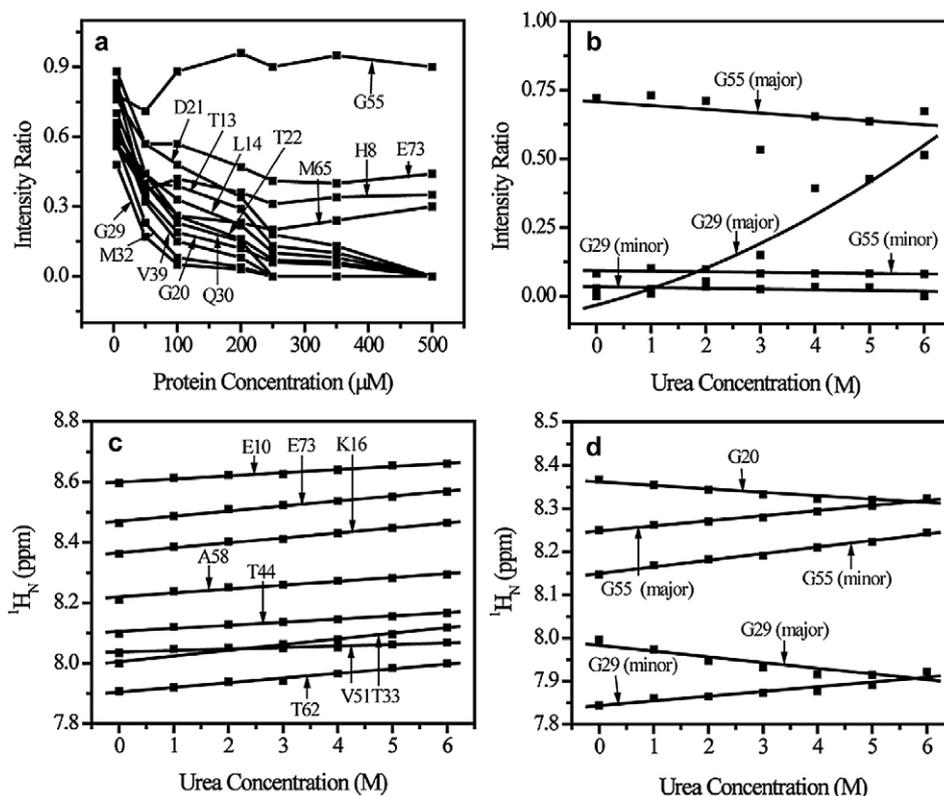
Fig. 8. Changes in intensity ratio and amide chemical shifts of cross-peaks in the 2D ^1H_N–^{15}N HSQC spectra recorded for SNase79 at different protein and urea concentrations, respectively. (a) Concentration dependence of intensity ratio of cross-peaks for residues in different structural regions. (b) Urea-induced changes in intensity ratio of major and minor cross-peaks of G29 and G55. (c) Urea-induced changes in amide chemical shifts for residues in different secondary structural regions. (d) Urea-induced changes in amide chemical shifts for cross-peak G20 and for major and minor cross-peaks of residues G29 and G55.

third position of the β-turn sequence. The replacement of G29 and G20 by V29 and V20, respectively, may prevent the segment T13–V39 of [G20V/G29V]SNase79 to from a native-like β-sheet conformation, which accounts for the self-association of fragment SNase79 at high concentration. Therefore, SNase79 may have some residual turn-like conformation.

The previous study revealed the doubling cross-peaks with unequal intensities for residues E10, G29, and G55 in the 2D ^1H_N–^{15}N HSQC spectra of SNase79, which is correlated with the cis/trans heterogeneity of X-prolyl peptide bonds in SNase79. The major cross-peak of G29, representing the native trans-form of X-prolyl bond Q30–P31, characterizes a high population of SNase79 having a native-like β-sheet conformation in the segment T13–V39. A small population of SNase79 displaying a minor cross-peak of G29 does not undergo self-association reaction [10]. Urea-denaturation experiments performed on 400 µM SNase79 provided downfield shifts of ^1H_N resonances for almost all cross-peaks including those for vast majority residues in self-association interface while urea concentrations were increased from 0 to 6.0 M (Fig. 8c). Both major and minor cross-peaks for residues E10 and G55 showed downfield shifts of ^1H_N resonances on increasing urea concentration (Fig. 8d, the data for E10 not shown). However, the upfield and downfield shifts of ^1H_N resonances were observed for major and minor cross-peaks of G29, respectively. The major and minor cross-peaks of G29 were gradually close up to each other in the ^1H_N chemical shifts on increasing the urea

concentrations and merged into a single cross-peak at 6.0 M urea (Fig. 8d). Similar upfield shift of ^1H_N resonance was observed also for G20 (Fig. 8d).

The upfield shift of ^1H_N resonance on increasing the urea concentration usually is a consequence of weakened hydrogen bonding. Therefore, some relevant conformational restriction may be imposed on G29 of SNase79 exhibiting high population, which makes the ^1H_N of G29 forming a hydrogen bond with the C=O of some residue or other in this localized structural region. The measurements of ^1H_N temperature coefficients give evidence of the involvement in intramolecular hydrogen bonding of residue G29 in monomeric SNase79. Thus, weakening the hydrogen bonding of G29 under the urea-denaturation interaction can release SNase79 from aggregation. In consequence, not only the ^1H_N resonance of major cross-peak of G29 tends to move upfield and merge with those of minor cross-peak (Fig. 8d), but also the intensity of major cross-peak of G29 is increased (Fig. 8b). This explains why the intensity of major cross-peak for G29 was increased dramatically, but those of minor cross-peak for G29 and doubling cross-peaks for G55 and E10 showed only slight changes on increasing the urea concentrations (Fig. 8b, the data for E10 not shown).

The interpretation for upfield shift of the major cross-peak of G29 can be applied also to cross-peak of G20 of SNase79 exhibiting high population. The monomeric state of [G20V/G29V]SNase79 at concentration of 500 µM provides the evi-

dence that the above described spectral phenomenon for doubling cross-peaks of G29 is caused by the residual turn conformation, but is not induced by aggregation of SNase79 at concentration of 400 μM. Therefore, the monomeric SNase79 has residual native-like β-turn structures which provide the conformational restrictions for G29 and G20.

3.6. Intermediate exchange motions correlated to residual structures

^{15}N relaxation parameters can indicate the conformational flexibility along the protein backbone. Negative ^{1}H–^{15}N NOEs were observed for almost all the detected residues of SNase79 (data not shown). ^{15}N relaxation rates R_1 and R_2 and the variation of R_2:R_1 ratios along the sequence of SNase79 are shown in Fig. 9. The explicit sequence-dependent variation of ^{15}N transverse relaxation rate (R_2) for both 50 μM SNase79 in aqueous solution and 400 μM SNase79 in 4.0 M urea were observed. A subset of residues of 50 μM SNase79, G20, D21, V23, G29, and M32, showed R_2:R_1 ratios (>4.8) greater than the average value of 3.57±1.24 (Fig. 9c). 400 μM SNase79 in 4.0 M urea provided the R_2:R_1 ratios (>3.8) higher than the average value of 2.57±0.91 for residues V23, Y27, G29, and M32 (Fig. 9f). The residues having relatively large R_2:R_1 ratios in both cases are within the self-association region of SNase79, particularly around two native-like β-turn regions. However, the self-association reaction of SNase79 was essentially excluded under both sample conditions. This was evidenced by experiments with SNase79 performed at different protein concentrations and at different urea concentrations (Fig. 8a, c). The large R_2 values for these residues (Fig. 9b, e) were obtained without a concomitant decrease in R_1 values of the corresponding residues (Fig. 9a, d). Therefore, the large deviations of R_2:R_1 ratios from the average values for the subset residues (Fig. 9c, f) were not caused by the aggregation-induced line broadening and motional anisotropy, but attributed to contributions from backbone mobility on ms-μs timescale [27]. Relatively high R_2:R_1 ratios (>4.0) were obtained also for residues S59, T62, M65, and V66 within the residual helix region of 50 μM SNase79 (Fig. 9c), but not for corresponding residues of 400 μM SNase79 in 4.0 M urea (Fig. 9f). The intermediate exchange motions on ms-μs timescale were not observed also for 400 μM SNase79 in 6.0 M urea and 500 μM [G20V/G29V]SNase79 in aqueous solution (data not shown). It may be because of that 4.0 M urea may disorder the residual helical conformation in SNase79 and 6.0 M urea can fully unfold the fragment, whereas [G20V/G29V]SNase79 may not have the residual β-turn conformations. Therefore, the observed intermediate exchange motions on ms–μs timescale are supposed to correlate with residual β-turn and helix structures of monomeric SNase79.

4. Discussion

4.1. Ensemble of highly heterogeneous conformations of SNase79

The secondary structure content of the segment spanning residues 1–79 of native SNase is 15.2%, 31.6%, and 10.1% for helix, β-sheets, and β-turn, respectively, according to the native structural elements from full-length protein. The CD and fluorescence data reveal the residual helix, turn or β-sheet secondary structures in monomeric SNase79, which is supported further by NMR data. The NMR derived $^{3}J_{NH–H\alpha}$ cou-

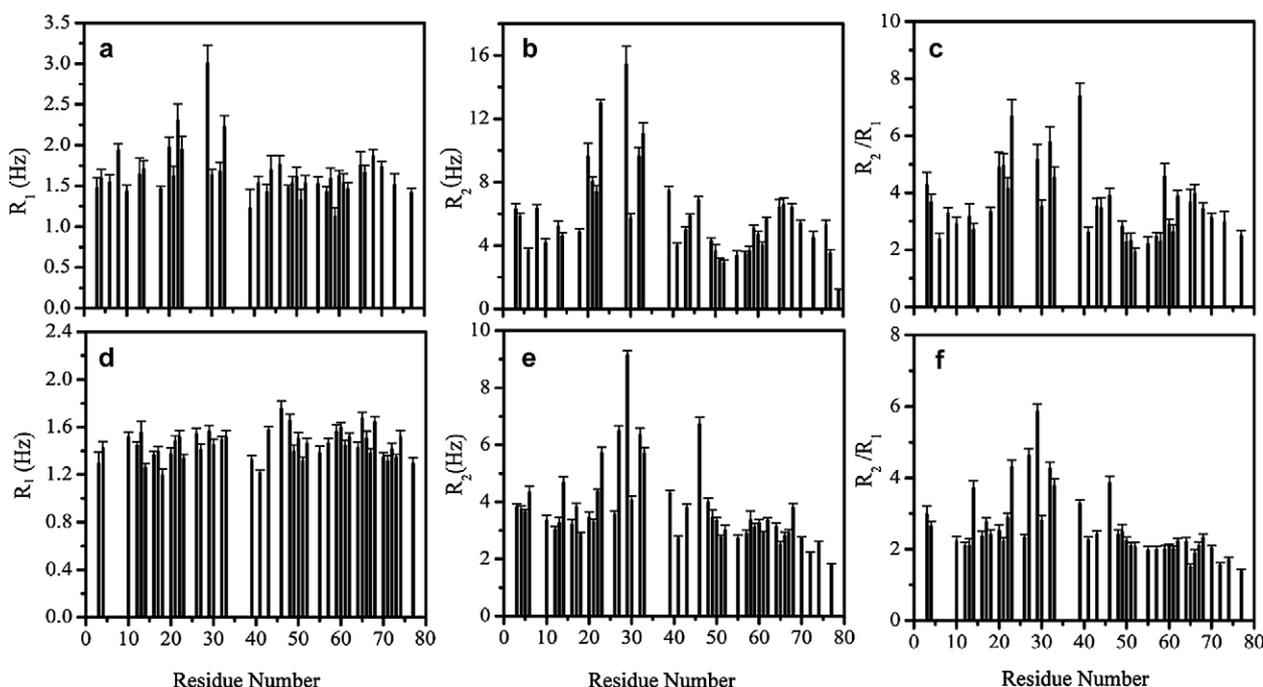Fig. 9. ^{15}N relaxation rates R_1 and R_2 and R_2ÓR_1 ratios. (a), (b), and (c) were obtained for 50 μM SNase79 in aqueous solution; (d), (e), and (f) for 400 μM SNase79 in 4.0 M urea.

pling constants, amide-proton temperature coefficients, $^{13}C_\alpha$ secondary chemical shifts, and NOE connectivities as well as the urea-denaturation and ^{15}N relaxation data characterize the potential helix and β-sheet or β-turn conformations in SNase79. The self-association effects on the data used for analysis can be excluded as described in Section 3.

SNase79 can be represented as an ensemble of interconverting conformations. A mixture of conformations including residual random-coil and helix as well as β-sheet structures was determined for monomeric SNase79 by CD spectra. The intermediate exchange motions of the segments of β-turn and helix α_1 regions of monomeric SNase79 were detected by ^{15}N relaxation experiments. Therefore, monomeric SNase79 is in a transient equilibrium involving a number of interconverting β-sheet-, helix- or turn-containing species and unfolded states. Previous study [10] has revealed the conformational heterogeneity of SNase79, showing two different populations in the ensemble of conformations. The piece of highly populated SNase79 exhibiting a native *trans*-form of Q30–P31 bond adopts native-like β-sheet conformation in the segment T13–V39, whereas SNase79 of low population having a nonnative *cis*-form of Q30–P31 bond shows nonnative conformation in the segment T13–V39. In addition, the minor *cis*- and major *trans*-forms of X-prolyl bonds E10–P11 and G55–P56 exist in both species of SNase79. The helix-like and β-sheet- or turn-like conformations may transiently populate in the ensemble of these heterogeneous conformations. Therefore, the conformational ensemble of SNase79 is a highly heterogeneous collection of interconverting conformations having transiently populated helix-like and β-sheet- or turn-like structures.

4.2. Localized structural propensities of SNase79

The residual structures of SNase79 have been detected by various biophysical methods in this study. The $^3J_{NH–H\alpha}$ coupling constants, amide-proton temperature coefficients, $^{13}C_\alpha$ secondary chemical shifts, ^{15}N relaxation rates, and urea-induced changes in ^1H_N chemical shifts indicate repeatedly the deviations from random coil values for two sequence regions of SNase79.

The first sequence region of SNase79 exhibiting non-random conformation contains residues K16, A17, I18, G20, D21, V23, Y27, G29, and M32 which are located in the β_I-sheet structural region for native SNase. The significant deviations of $^3J_{NH–H\alpha}$ coupling constants for these residues from the values obtained in random-coil model suggest the structural preference for β-sheet-like conformation of the corresponding segment. The lowered amide-proton temperature coefficients for residues I18, D21, T22, V23, G29, Q30, and T33 provide the strong evidence that the amide protons of these residues are relatively protected from exchange with solvent, presumably as a result of intramolecular hydrogen-bonding in β-sheet-like structure of this region in SNase79. The uncommon upfield shift of ^1H_N resonances for G20 and G29 induced by urea-denaturation reaction reveal the localized conformational preferences for native-like β-turn τ_1 and τ_2 structures in SNase79

which determine the extended β-sheet-like conformation in SNase79.

The second sequence region of SNase79 having non-random conformation involves some residues in segment A58–A69, which show the explicit tendency to form α-helical-like conformation in the fragment. The positive $^{13}C_\alpha$ secondary chemical shifts, below-average $^3J_{NH–H\alpha}$ coupling constants, and lowered amide-proton temperature coefficients for residues, A58, A60, F61, T62, M65, and V66 provide the conclusive evidences of the localized conformational preference for α-helical structure in this region.

As indicated above, the oligomerization effects on the NMR data obtained for SNase79 can be excluded. Therefore, the localized conformational preferences for helix-, β-sheet- and especially turn-like structures in the sequence regions T13–V39 and A58–A69 of SNase79 are not induced by aggregation, but intrinsic to the monomer of SNase79. The determined intrinsic propensities towards residual secondary structures are significant for the conformational ensemble of SNase79.

4.3. Intrinsic interactions for structure-forming tendencies of SNase79

The intrinsic propensity for turn-like structures of segments I18–D21 and Y27–Q30 is determined by the intrinsic local interactions in these two regions. Disruption of these intrinsic local interactions in the two β-turn regions by G20V/G29V double mutation produces a monomeric [G20V/G29V] SNase79 of high concentration. SNase79, having nonnative *cis*-conformation of Q30–P31 bond does not undergo self-association reaction [10]. The *cis*-form of Q30–P31 bond may cause some localized interactions other than these intrinsic local interactions in the corresponding turn region of SNase79. Therefore, these two turn regions can be regarded as the potential initiation sites in the folding of SNase79. The intrinsic propensity for turn-like structures of segments I18–D21 and Y27–Q30 of SNase79, originating from intrinsic local interactions, is a significant determinant of these potential initiation sites.

The unstable β_I-sheet-like folding of the segment T13–V39 can account for the strong tendency to aggregate of SNase79. However, SNase36 containing entire sequence of β_I-sheet structure showed no tendency to self-aggregation. The conformational ensemble of SNase36 adopts mainly a transient population of turn-like conformations [4]. This suggests that the intrinsic non-local interactions for forming β_I-sheet-like structure exist in the segment T13–V39 of SNase79, which may act as a potential non-local initiation site in the folding of SNase79. SNase110 encompasses all residues from β_I- and β_{II}-sheets in the "β-barrel" region of native SNase, and the non-local interactions in the β-barrel-like region of SNase110 drives the fragment to be in a partially folded state [5]. However, the intrinsic native-like long-range interactions between residues from β_I- and β_{II}-sheets does not exist in SNase79 compared with SNase110, owing to the incompleteness of SNase79 in the sequence region of β_{II}-sheet. This is proved by the V66W

single mutation of SNase fragments. V66W single mutation can facilitate the 110-residue SNase fragment to fold into a native-like tertiary conformation [5]. Nevertheless, V66W mutation of SNase79 cannot stabilize the β_I-sheet-like folding, thus cannot prevent the aggregation of the fragment at high concentration. In view of this, the intrinsic non-local interactions for β_I-sheet structural region are insufficient to account for stabilizing the β_I-sheet structure in the absence of the interactions with residues from β-strands constructing β_{II}-sheet in SNase79.

It was proposed that the α-helix is a favorite candidate for folding initiation sites in protein folding. The localized propensity for helical-like structure is determined for residues A58–A69 of SNase79. Thus, Residues A58–A69, forming helix α_1 in native SNase, could act as a local folding nucleation site in SNase79. However, the intrinsic local interactions in the segment A58–A69 appear to be insufficient to stabilize this helical conformation in the absence of other interactions, such as the long-range interactions with β-strands in SNase79. This was demonstrated by V66W mutation of SNase fragments. The V66W single mutation of SNase110 can trigger the fragment to fold into a native-like tertiary conformation [5]. However, due to a shortage of long-range tertiary interactions displayed in SNase110, V66W79 exhibits the similar behaviors to those of SNase79. Therefore, the existing local intrinsic interactions in the segment A58–A69 only can trigger the formation of a very fluctuating helical-like structure in SNase79.

In summary, the identified intrinsic propensities for secondary structure formation can reflect the localized intrinsic interactions in SNase79, but is not the result of stabilizing intermolecular interactions by oligomerization effects. The intrinsic local and non-local interactions in the potential local and non-local initiation sites of SNase79 are insufficient to stabilize the folding of the fragment due to the absence of relevant long-range interactions. In consequence, SNase79 shows a highly heterogeneous collection of interconverting conformations having transiently populated helix-like and β-sheet- or turn-like structures.

Acknowledgements

Annexe A. Supplementary data

Supplementary data associated with this article can be found, in the online version, at doi: (10.1016/j.biochi.2006.05.002).

References

[1] G. De Prat Gay, J. Ruiz-Sanz, J.L. Neira, L.S. Itzhaki, A.R. Fersht, Folding of a nascent polypeptide chain in vitro: cooperative formation of structure in a protein module, Proc. Natl. Acad. Sci. USA 92 (1995) 3683–3686.

[2] G. De Prat Gay, J. Ruiz-Sanz, J.L. Neira, F.J. Corrales, D.E. Otzen, A.G. Ladurner, A.R. Fersht, Conformational pathway of the polypeptide chain of chymotrypsin inhibitor-2 growing from its N terminus in vitro. Parallels with the protein folding pathway, J. Mol. Biol. 254 (1995) 968–979.

[3] J.L. Neira, A.R. Fersht, Exploring the folding funnel of a polypeptide chain by biophysical studies on protein fragments, J. Mol. Biol. 285 (1999) 1309–1333.

[4] J. Dai, X. Wang, Y. Feng, G. Fan, J. Wang, Searching for folding initiation sites of staphylococcal nuclease: a study of N-terminal short fragments, Biopolymers 75 (2004) 229–241.

[5] Y. Feng, D. Liu, J. Wang, Native-like partially folded conformations and folding process revealed in the N-terminal large fragments of staphylococcal nuclease: a study by NMR spectroscopy, J. Mol. Biol. 330 (2003) 821–837.

[6] K. Ye, G. Jing, J. Wang, Interactions between subdomains in the partially folded state of staphylococcal nuclease, Biochim. Biophys. Acta 1479 (2000) 123–134.

[7] Y. Wang, D. Shortle, A dynamic bundle of four adjacent hydrophobic segments in the denatured state of staphylococcal nuclease, Protein Sci. 5 (1996) 1898–1906.

[8] A.T. Alexandrescu, A.G. Gittis, C. Abeygunawardana, D. Shortle, NMR structure of a stable "OB-fold" sub-domain isolated from staphylococcal nuclease, J. Mol. Biol. 250 (1995) 134–143.

[9] J. Wang, D.M. Truckses, F. Abildgaard, Z. Dzakula, Z. Zolnai, J.L. Markley, Solution structures of staphylococcal nuclease from multidimensional, multinuclear NMR: nuclease-H124L and its ternary complex with Ca^{2+} and thymidine-3',5'-bisphosphate, J. Biomol. NMR 10 (1997) 143–164.

[10] X. Wang, Y. Tong, J. Wang, Cis/trans heterogeneity of Gln30–Pro31 peptide bond determines whether a 79-residue fragment of staphylococcal nuclease self-associates, Biochem. Biophys. Res. Commun. 329 (2005) 495–501.

[11] A. Hemsley, N. Arnheim, M.D. Toney, G. Cortopassi, D.J. Galas, A simple method for site-directed mutagenesis using the polymerase chain reaction, Nucleic Acids Res. 17 (1989) 6545–6551.

[12] M.R. Eftink, C.A. Ghiron, Fluorescence quenching studies with proteins, Anal. Biochem. 114 (1981) 199–227.

[13] J.L. Markley, A. Bax, Y. Arata, C.W. Hilbers, R. Kaptein, B.D. Sykes, P.E. Wright, K. Wuthrich, Recommendations for the presentation of NMR structures of proteins and nucleic acids. IUPAC-IUBMB-IUPAB Inter-Union Task Group on the standardization of data bases of protein and nucleic acid structures determined by NMR spectroscopy, J. Biomol. NMR 12 (1998) 1–23.

[14] I. Baskakov, D.W. Bolen, Forcing thermodynamically unfolded proteins to fold, J. Biol. Chem. 273 (1998) 4831–4834.

[15] L. Stryer, The interaction of a naphthalene dye with apomyoglobin and apohemoglobin. A fluorescent probe of non-polar binding sites, J. Mol. Biol. 13 (1965) 482–495.

[16] G.V. Semisotnov, N.A. Rodionova, O.I. Razguyaev, U.V. Ucersky, A. Gripas, R.I. Grilmanshin, Study of the "molten globule" intermediate state in protein folding by a hydrophobic fluorescent probe, Biopolymers 31 (1991) 119–128.

[17] K. Tian, B. Zhou, F. Geng, G. Jing, Folding of SNase R begins early during synthesis: the conformational feature of two short N-terminal fragments of staphylococcal nuclease R, Int. J. Biol. Macromol. 23 (1998) 199–206.

[18] L.J. Smith, K.A. Bolin, H. Schwalbe, M.W. MacArthur, J.M. Thornton, C.M. Dobson, Analysis of main chain torsion angles in proteins: prediction of NMR coupling constants for native and random coil conformations, J. Mol. Biol. 255 (1996) 494–506.

[19] A.E. Meekhof, S.M. Freund, Probing residual structure and backbone dynamics on the milli- to picosecond timescale in a urea-denatured fibronectin type III domain, J. Mol. Biol. 286 (1999) 579–592.

[20] T.G. Pedersen, B.W. Sigurskjold, K.V. Andersen, M. Kjaer, F.M. Poulsen, C.M. Dobson, C. Redfield, A nuclear magnetic resonance

study of the hydrogen-exchange behaviour of lysozyme in crystals and solution, J. Mol. Biol. 218 (1991) 413–426.

[21] N.J. Baxter, L.L. Hosszu, J.P. Waltho, M.P. Williamson, Characterisation of low free-energy excited states of folded proteins, J. Mol. Biol. 284 (1998) 1625–1639.

[22] J. Juneja, N.S. Bhavesh, J.B. Udgaonkar, R.V. Hosur, NMR identification and characterization of the flexible regions in the 160 kDa molten globule-like aggregate of barstar at low pH, Biochemistry 41 (2002) 9885–9899.

[23] G. Merutka, H.J. Dyson, P.E. Wright, 'Random coil' 1H chemical shifts obtained as a function of temperature and trifluoroethanol concentration for the peptide series GGXGG, J. Biomol. NMR 5 (1995) 14–24.

[24] J.F. Wang, A.P. Hinck, S.N. Loh, J.L. Markley, Two-dimensional NMR studies of staphylococcal nuclease. 2. Sequence-specific assignments of carbon-13 and nitrogen-15 signals from the nuclease H124L-thymidine 3',5'-bisphosphate-Ca^{2+} ternary complex, Biochemistry 29 (1990) 102–113.

[25] D.S. Wishart, B.D. Sykes, Chemical shifts as a tool for structure determination, Methods Enzymol. 239 (1994) 363–392.

[26] D.S. Wishart, B.D. Sykes, F.M. Richards, Relationship between nuclear magnetic resonance chemical shift and protein secondary structure, J. Mol. Biol. 222 (1991) 311–333.

[27] G. Barbato, M. Ikura, L.E. Kay, R.W. Pastor, A. Bax, Backbone dynamics of calmodulin studied by 15N relaxation using inverse detected two-dimensional NMR spectroscopy: the central helix is flexible, Biochemistry 31 (1992) 5269–5278.